Efficient Second-Order Strang Splitting Scheme with Exponential Integrating Factor for the Scalar Allen-Cahn Equation

Chunya Wu, Yuting Zhang, Danchen Zhu, Ying Ye, Lingzhi Qian*

***Abstract*—An efficient and easy-to-implement second-order Strang splitting approach is mainly applied to study the scalar Allen-Cahn (AC) equation in this paper. Base on the idea of dimensional splitting, a new time dependent function (called exponential integrating factor) is introduced for the scalar AC equation. Then we propose the Strang splitting approach which is aim to decompose the original equation into linear part and nonlinear part. In particular, the explicit 2-stage strong stability preserving Runge-Kutta(SSP-RK2) method is employed for the nonlinear part. Furthermore, we rigorously demonstrate the maximum principle, energy stability and convergence of the proposed scheme. Various numerical simulations in 2D and 3D are presented to confirm the validity of the proposed method.**

***Index Terms*—Strang splitting, Exponential integrating factor, Maximum principle, Energy stability, Convergence.**

I. Introduction

IN this paper, we mainly focus on the following scalar AC equation[1]

$$\begin{cases} \partial_t u = \varepsilon^2 \Delta u - f(u), \quad (t, \mathbf{x}) \in (0, \infty) \times \Omega \\ F'(u) = f(u), \\ u\big|_{t=0} = u^0, \end{cases} \tag{1}$$

where u is a real-valued function, ε^2 is the mobility coefficient, and $F(u) = \frac{1}{4}(u^2 - 1)^2$ means the standard double potential. It is well known that the scalar Allen-Cahn equation can be regarded as the L^2-gradient flow of the free energy function $E(u)$,

$$E(u) = \int_\Omega \left(\frac{\varepsilon^2}{2} |\nabla u|^2 + F(u) \right) d\mathbf{x}, \tag{2}$$

and for smooth solutions of the equation (1), it is easy to obtain the total energy $E(u)$ is non-increasing in time, i.e., $\frac{d}{dt} E(u) \leq 0$.

Up to now, there have been great deal of researches on both numerical and mathematical analysis aspects for the scalar AC equation[3], [19]. Du et.al proposed integrating factor Runge-Kutta method to solve a few classical semi-parabolic equations, and proved the maximum principle preserving and energy stability of the presented scheme[6]. Shen et.al considered the maximum principle preserving of the implicit-explicit scheme for the generalized AC equation[9]. Zhang et.al provided and analyzed a class of up to fourth order maximum principle preserving integrators for the AC equation[21]. In addition, many approaches have been done for solving the scalar AC equation, such as implicit or explicit scheme[16], exponential time difference(ETD) scheme[4] , scalar auxiliary variables(SAV) approach[10], and Strang splitting method[5], [7], [8], [11], [12], [13], [14], [15], [17], [18], [20] etc. In this paper, we mainly consider the Strang splitting to solve the scalar AC equation. The Strang splitting is a typical operator splitting method, which mainly decompose the complex original problem into two simple sub-problems, so as to making the problem easier and more effective. The standard form of Strang splitting method is given by

$$u^{n+1} = \mathcal{S}_L(\frac{\tau}{2}) \mathcal{S}_N(\tau) \mathcal{S}_L(\frac{\tau}{2}) u^n, \tag{3}$$

where $\tau > 0$ is the time step, $\mathcal{S}_L$ and $\mathcal{S}_N$ denote the linear part and nonlinear part, respectively.

However, to the best of our knowledge, there is limited work for the Strang splitting method with exponential integrating factor for the scalar AC equation. What is more, because of the high dimensionality, stiffness of the diffusion and reaction terms and nonlinearity of the function $F(u)$, the numerical study of the AC equation is still challenging. In addition, if the initial data is not smooth enough or incompatible with the boundary value, spurious oscillations in the numerical solution might occur. Therefore, in this paper, we adopt the idea of dimensional splitting to incorporate the exponential integrating factor[2]. And in order to establish an effective and easy-to-implement second-order scheme for solving the scalar AC equation in 2D and 3D, we employ the second order central finite difference method for spatial discretization and the Strang splitting approach for temporal discretization. The most important purpose of using the Strang splitting is to divide the original problem into the linear part and nonlinear part. The nonlinear part mainly is solved by SSP-RK2 approach and the linear part is solved analytically. In addition, the maximum principle, energy stability and convergence of the presented scheme are proved. In the last but no least, through the aid of numerical simulations in 2D and 3D, we verify our theoretical results and illustrate the effectiveness of the presented scheme.

The rest part of this paper is organized as follows. In Section II, we illustrate how the problem is discretized

Manuscript received August 8, 2022; revised January 19, 2023. This work was supported in part by the the NSF of China (No. 11861054), Natural Science Foundation of Guangxi (No. 2020GXNSFAA297223), English curriculum construction project of Guangxi Normal University (No. 2021XJQYW04)

Chunya Wu is a graduate student of the Guangxi Normal University, Guilin Guangxi 541000, P.R. China (e-mail:chunyawu00@stu.gxnu.edu.cn).

Yuting Zhang is a graduate student of the Guangxi Normal University, Guilin Guangxi 541000, P.R. China (e-mail:zhangyuting@stu.gxnu.edu.cn‘).

Danchen Zhu is a graduate student of the Guangxi Normal University, Guilin Guangxi 541000, P.R. China (e-mail:zhudanchen@stu.gxnu.edu.cn).

Ying Ye is a graduate student of the Guangxi Normal University, Guilin Guangxi 541000, P.R. China (e-mail:yeying@stu.gxnu.edu.cn).

*Lingzhi Qian is an associate professor of the College of Mathematics and Statistics in Guangxi Normal University, Guilin 541006, P.R. China(corresponding author, e-mail: qianlz@mailbox.gxnu.edu.cn).

in time, and how to use the exponential integrating factor approach for the multidimensional AC equation. In Section III, the maximum principle, energy stability and convergence are studied for this method. Various numerical experiments in 2D and 3D are performed by Section IV. Finally, conclusions are given in Section V.

II. An effective and easy-to-implement second-order scheme

A. The exponential integrating factor method

For the equation (1), we can approximate the operator $L = -\varepsilon^2\Delta$ with periodic, Neumann or Dirichlet conditions in multi-dimension. Let h be an equidistant grid size, p denotes the number of spatial grid points along each direction and I_p is an identity matrix. Then

$$L_p = -\frac{\varepsilon^2}{h^2}\begin{pmatrix} -2 & b & & & c \\ 1 & -2 & 1 & & \\ & \ddots & \ddots & \ddots & \\ & & 1 & -2 & 1 \\ c & & & b & -2 \end{pmatrix} \tag{4}$$

When $b = 1$, $c = 0$ or $c = 1$, the matrix (4) is corresponding the homogeneous Dirichlet and periodic boundary conditions, respectively. When $c = 0, b = 2$, the matrix (4) is corresponding the homogeneous Neumann condition. Therefore, we can conclude that:
In 1D case, the approximation of L is derived from $L = L_1$ with $L_1 = L_p$.
In 2D case, L is given by $L = L_1 + L_2$ with $L_1 = I_p \otimes L_p$ and $L_2 = L_p \otimes I_p$.
Similarly, in 3D case, $L = L_1 + L_2 + L_3$ with $L_1 = I_p \otimes I_p \otimes L_p$, $L_2 = I_p \otimes L_p \otimes I_p$ and $L_3 = L_p \otimes I_p \otimes I_p$.
Remark 1: We can easily extend to higher dimensions $L = \sum_{i=1}^{d} L_i$ with

$$L_i = \underbrace{I_p \otimes \cdots I_p}_{(d-i)times} \otimes \underbrace{L_p}_{pos(d-i+1)} \otimes \underbrace{I_p \otimes \cdots \otimes I_p}_{(i-1)times} \tag{5}$$

Then, the equation (1) can be rewritten as

$$\partial_t \mathbf{U} + L\mathbf{U} = N(\mathbf{U}), \tag{6}$$

where $N(\mathbf{U}) = -f(\mathbf{U})$.

Now, a new time dependent function with exponential integrating factor of the form $W = e^{L_1 t}\mathbf{U}$ is given. We first consider the 2D case $L = L_1 + L_2$ for the equation (6). The derivative with respect to time t of W is

$$W_t = e^{L_1 t}\mathbf{U}_t + L_1 e^{L_1 t}\mathbf{U}. \tag{7}$$

Then, according to the equation (7) and following that L_1 and $e^{L_1 t}$ commute, we derive

$$W_t = e^{L_1 t}N(e^{-L_1 t}W) - L_2 W, \tag{8}$$

with the initial value $W(0) = e^{L_1 0}\mathbf{U}^0 = \mathbf{U}^0$.
Remark 2: Similarly, the solution of (7) with $L = \sum_{i=1}^{d} L_i$ can be given in higher dimension by

$$V_t = g(V) - L_d V, \ V(0) = \mathbf{U}^0 \tag{9}$$

where $g(V) = (e^{L_{d-1}t} \bullet \cdots \bullet e^{L_1 t})N((e^{-L_1 t} \bullet \cdots \bullet e^{-L_{d-1}t})V)$ and $\bullet$ is the matrix multiplication.

B. The Strang splitting in time

In this subsection, we will focus on the Strang splitting for the equation (8). Firstly, we denote by $\mathcal{S}_L$ and $\mathcal{S}_N$ are the exact solution operators associated with the linear and nonlinear part, respectively.

$$\mathcal{S}_L : W_t = -L_2 W. \tag{10}$$

$$\mathcal{S}_N : W_t = e^{L_1 t}N(e^{-L_1 t}W). \tag{11}$$

Then, we can approximate the solution W^{n+1} of the subproblem (10),

$$\mathcal{S}_L : W^{n+1} = e^{-L_2\tau}W^n. \tag{12}$$

And we adopt the SSP-RK2 method to solve the nonlinear part $\mathcal{S}_N$,

$$\begin{cases} W^* = W^n + \tau e^{L_1\tau}N(e^{-L_1\tau}W^n), \\ W^{n+1} = \frac{1}{2}W^* + \frac{1}{2}W^n + \frac{1}{2}\tau e^{L_1\tau}N(e^{-L_1\tau}W^*). \end{cases} \tag{13}$$

In summary, according to the standard Strang splitting (3), the effective and easy-to-implement second order scheme is derived as follows,

$$\begin{cases} W^{n,1} = e^{-L_2\frac{\tau}{2}}W^n, \\ W^{n,2} = W^{n,1} + \tau e^{L_1\tau}N(e^{-L_1\tau}W^{n,1}), \\ W^{n,3} = \frac{1}{2}W^{n,1} + \frac{1}{2}W^{n,2} + \frac{1}{2}\tau e^{L_1\tau}N(e^{-L_1\tau}W^{n,2}), \\ W^{n+1} = e^{-L_2\frac{\tau}{2}}W^{n,3}. \end{cases} \tag{14}$$

Using the exponential integrating factor $\mathbf{U} = e^{-L_1 t}W$, we obtain the numerical solution $\mathbf{U}^{n+1}$.

In particular, following the similar steps above, one can obtain the second-order scheme for the scalar AC equation in 3D case

$$\begin{cases} V^{n,1} = e^{-L_3\frac{\tau}{2}}V^n, \\ V^{n,2} = V^{n,1} + \tau e^{L_2\tau}e^{L_1\tau}N(e^{-L_2\tau}e^{-L_1\tau}V^{n,1}), \\ V^{n,3} = \frac{1}{2}V^{n,1} + \frac{1}{2}V^{n,2} + \frac{1}{2}\tau e^{L_2\tau}e^{L_1\tau}N(e^{-L_2\tau}e^{-L_1\tau}V^{n,2}), \\ V^{n+1} = e^{-L_3\frac{\tau}{2}}V^{n,3}, \end{cases} \tag{15}$$

where $V(t) = e^{L_2 t}W(t)$.
Remark 3: It is easy to find that the proposed scheme is highly efficient and easy-to-implement, which is an explicit method and only needs to solve some purely linear equations at each time step. Owing to the exponential matrix is dense in high spatial dimensions, if we directly calculate the exponential matrix, it will cause highly computational prices. Thus, the second-order approximation of the matrix exponential mainly employ the rational approximation[2]. It will greatly reduce the amount of computation and increase the speed of calculation.

III. The maximum principle, energy stability and convergence

In this section, we discuss the properties of the scheme (14), including the maximum principle, the stability of the discrete energy and convergence.
Theorem 3.1[6](Maximum principle) For any $0 < \tau \le \frac{1}{2}$ and any $n \ge 0$, assuming that $\|\mathbf{U}^n\|_\infty \le 1$ and $i > 0$. It follows that

$$\|\mathbf{U}^{n+1}\|_\infty \le 1. \tag{16}$$

Proof. Utilizing $W = e^{L_1 t}\mathbf{U}$, L_1 and L_2 are the positive definite matrix, we derive

$$\begin{aligned}
\left\|\mathbf{U}^{n,1}\right\|_\infty &= \left\|e^{-L_2\frac{\tau}{2}}e^{-iL_1\frac{\tau}{2}}\mathbf{U}^n\right\|_\infty \le \mathbf{U}_*,\\
\left\|\mathbf{U}^{n,2}\right\|_\infty &= \left\|e^{-iL_1\tau}\mathbf{U}^{n,1} + \tau e^{-iL_1\tau}N(\mathbf{U}^{n,1})\right\|_\infty\\
&\le \left\|e^{-iL_1\tau}\right\|_\infty \left\|\mathbf{U}^{n,1} + \tau N(\mathbf{U}^{n,1})\right\|_\infty \le \mathbf{U}_*,\\
\left\|\mathbf{U}^{n,3}\right\|_\infty &= \left\|\frac{1}{2}e^{-iL_1\tau}\mathbf{U}^{n,1} + \frac{1}{2}e^{-iL_1\tau}\mathbf{U}^{n,2} + \frac{1}{2}\tau e^{-iL_1\tau}N(\mathbf{U}^{n,2})\right\|_\infty\\
&\le \mathbf{U}_*,\\
\left\|\mathbf{U}^{n+1}\right\|_\infty &= \left\|e^{-L_2\frac{\tau}{2}}e^{-iL_1\frac{\tau}{2}}\mathbf{U}^{n,3}\right\|_\infty \le \mathbf{U}_*,
\end{aligned}$$

which completes the proof.

Theorem 3.2(Energy stability) Assume that the initial value $\|\mathbf{U}^0\|_\infty \le 1$. For the standard double potential $F(u)$, and under the time steps constraint $\tau \le 2$, the scheme (14) is long-time energy stability:

$$\tilde{E}^{n+1} - \tilde{E}^n \le 0. \tag{17}$$

Proof. Let $\tilde{\mathbf{U}}^n = \mathcal{S}_L(\frac{\tau}{2})\mathbf{U}^n$ and $\mathbf{U}^{n+1} = \mathcal{S}_L(\frac{\tau}{2})\mathcal{S}_N(\tau)\mathcal{S}_L(\frac{\tau}{2})\mathbf{U}^n$, we have

$$\tilde{\mathbf{U}}^{n+1} = \mathcal{S}_L(\tau)\mathcal{S}_N(\tau)\tilde{\mathbf{U}}^n. \tag{18}$$

This yields,

$$e^{L_2\tau}\tilde{\mathbf{U}}^{n+1} = \mathcal{S}_N(\tau)\tilde{\mathbf{U}}^n, \tag{19}$$

and due to the formula (13), we obtain

$$\mathcal{S}_N(\tau)\tilde{\mathbf{U}}^n = \tilde{\mathbf{U}}^n + \frac{1}{2}\tau N(\tilde{\mathbf{U}}^n) + \frac{1}{2}\tau N(\tilde{\mathbf{U}}^*) \le \tilde{\mathbf{U}}^n + \tau F'(\mathbf{z}^n), \tag{20}$$

where $F'(\mathbf{z}^n) = max\left\{N(\tilde{\mathbf{U}}^n), N(\tilde{\mathbf{U}}^*)\right\}$ and $F(\mathbf{z}) = -\frac{1}{4}(\mathbf{z}^2-1)^2$. Then we rewrite the formula (19) as

$$\frac{1}{\tau}(e^{L_2\tau}-1)\tilde{\mathbf{U}}^{n+1} + \frac{1}{\tau}(\tilde{\mathbf{U}}^{n+1} - \tilde{\mathbf{U}}^n) \le F'(\mathbf{z}^n). \tag{21}$$

Then, by taking the inner product of the first term on the right side in the above formula with $(\tilde{\mathbf{U}}^{n+1} - \tilde{\mathbf{U}}^n)$, we obtain

$$\begin{aligned}
&\frac{1}{\tau}\langle(e^{L_2\tau}-1)\tilde{\mathbf{U}}^{n+1}, \tilde{\mathbf{U}}^{n+1} - \tilde{\mathbf{U}}^n\rangle = \frac{1}{\tau}\langle(1-e^{-L_2\tau})\mathbf{U}^{n+1}, \mathbf{U}^{n+1} - \mathbf{U}^n\rangle\\
&= \frac{1}{2\tau}\langle(1-e^{-L_2\tau})\mathbf{U}^{n+1}, \mathbf{U}^{n+1}\rangle - \frac{1}{2\tau}\langle(1-e^{-L_2\tau})\mathbf{U}^n, \mathbf{U}^n\rangle\\
&+ \frac{1}{2\tau}\langle(1-e^{-L_2\tau})(\mathbf{U}^{n+1} - \mathbf{U}^n), (\mathbf{U}^{n+1} - \mathbf{U}^n)\rangle.
\end{aligned} \tag{22}$$

Multiplying (21) by $(\tilde{\mathbf{U}}^{n+1} - \tilde{\mathbf{U}}^n)$, and using the formula (22), we have

$$\begin{aligned}
\tilde{E}^{n+1} - \tilde{E}^n \le &-\frac{1}{2\tau}\langle(1-e^{-L_2\tau})(\mathbf{U}^{n+1} - \mathbf{U}^n), (\mathbf{U}^{n+1} - \mathbf{U}^n)\rangle\\
&-\langle(\frac{1}{\tau} - \frac{1}{2}F''(\xi^n))(\tilde{\mathbf{U}}^{n+1} - \tilde{\mathbf{U}}^n)^2, 1\rangle,
\end{aligned} \tag{23}$$

where ξ^n is some functions between $\tilde{\mathbf{U}}^n$ and $\tilde{\mathbf{U}}^{n+1}$, and $F''(\xi^n)$ is from as follows:

$$F(\tilde{\mathbf{U}}^{n+1}) = F(\tilde{\mathbf{U}}^n) + F'(\tilde{\mathbf{U}}^n)(\tilde{\mathbf{U}}^{n+1} - \tilde{\mathbf{U}}^n) + \frac{1}{2}F''(\xi^n)(\tilde{\mathbf{U}}^{n+1} - \tilde{\mathbf{U}}^{n-1})^2, \tag{24}$$

and it is not difficult to check that

$$F''(\xi^n) = 1 - 3(\xi^n)^2. \tag{25}$$

Then, when $\tau \le 2$,

$$\frac{1}{\tau} - \frac{1}{2}F''(\xi^n) \ge 0. \tag{26}$$

Thus we prove that $\tilde{E}^{n+1} - \tilde{E}^n \le 0$ for all $n \ge 0$.

Next, in order to prove the convergence of the proposed scheme, we first need to introduce some notes and results. For any functions $\mathbf{U} \in (0, T; H^s_{per}(\Omega))(s > 1)$. Let $\bar{\mathbf{U}}^k$ be the numerical solution of the scheme (14) at t_k, and $\mathbf{U}^k_e$ be the exact solution of the original equation (1) at t_k. Then we define a grid function space on Ω_h

$$w^h = \left\{\mathbf{U}|\mathbf{U} = \left\{\mathbf{U}_{i,j}|0 \le i, j \le N+1\right\}\right\}, \tag{27}$$

and a mapping $I^h : H^s_{per}(\Omega) \to w^h$ by $I^h(\mathbf{U}) = \mathbf{U}$, where $H^s_{per}(\Omega) = \{\mathbf{U} \in H^s(\Omega)|\mathbf{U}\ is\ \Omega - periodic\}$.

Lemma 3.1 For any function $\mathbf{U} \in w^h$, it holds that

$$\begin{aligned}
\left\|\mathcal{S}_L\mathbf{U}\right\| &\le \left\|\mathbf{U}\right\|,\\
\left\|\mathcal{S}_N\mathbf{U}\right\| &\le \left\|\mathbf{U}\right\|.
\end{aligned} \tag{28}$$

Lemma 3.2 For any function $\mathbf{U} \in w^h$, we obtain

$$\left\|(I^h\mathcal{S}_L - \mathcal{S}_L I^h)\mathbf{U}\right\| \le C_2 h^s\left|\mathbf{U}\right|_s, \tag{29}$$

where C_2 is a positive constant independent τ and h.

Lemma 3.3[18] For any function $\mathbf{U} \in w^h$, we obtain

$$\left\|(I^h\mathcal{S}_N - \mathcal{S}_N I^h)\mathbf{U}\right\| \le C_3\tau(\tau^2 + h^2 + \tau h^{2+s}), \tag{30}$$

where C_3 is a positive constant independent τ and h.

Theorem 3.4 Supposed $\mathbf{U} \in H^s_{per}(\Omega)$, then there exists a positive constant C independent of τ and h, such that

$$\left\|\mathbf{U}^{k+1} - I^h\mathbf{U}^{k+1}_e\right\| \le C(\tau^2 + h^2 + \tau h^{2+s} + \frac{h^s}{\tau}). \tag{31}$$

Proof. For $k > 0$, due to the Strang splitting approach is second order[5], [11], we have

$$\begin{aligned}
\left\|\mathbf{U}^{k+1} - I^h\mathbf{U}^{k+1}_e\right\| &\le \left\|\mathbf{U}^{k+1} - I^h\bar{\mathbf{U}}^{k+1}\right\| + \left\|I^h\bar{\mathbf{U}}^{k+1} - I^h\mathbf{U}^{k+1}_e\right\|\\
&\le \left\|\mathbf{U}^{k+1} - I^h\bar{\mathbf{U}}^{k+1}\right\| + C_1\tau^2.
\end{aligned} \tag{32}$$

Then, utilizing the lemma 3.2, we can derive

$$\begin{aligned}
&\left\|\mathbf{U}^{k+1} - I^h\bar{\mathbf{U}}^{k+1}\right\| = \left\|\mathcal{S}_L\mathcal{S}_N\mathcal{S}_L\mathbf{U}^k - I^h\mathcal{S}_L\mathcal{S}_N\mathcal{S}_L\bar{\mathbf{U}}^k\right\|\\
&\le \left\|\mathcal{S}_L\mathcal{S}_N\mathcal{S}_L\mathbf{U}^k - \mathcal{S}_L I^h\mathcal{S}_N\mathcal{S}_L\bar{\mathbf{U}}^k\right\|\\
&+ \left\|\mathcal{S}_L I^h\mathcal{S}_N\mathcal{S}_L\bar{\mathbf{U}}^k - I^h\mathcal{S}_L\mathcal{S}_N\mathcal{S}_L\bar{\mathbf{U}}^k\right\|\\
&= \left\|\mathcal{S}_L(\mathcal{S}_N\mathcal{S}_L\mathbf{U}^k - I^h\mathcal{S}_N\mathcal{S}_L\bar{\mathbf{U}}^k)\right\|\\
&+ \left\|(\mathcal{S}_L I^h - I^h\mathcal{S}_L)\mathcal{S}_N\mathcal{S}_L\bar{\mathbf{U}}^k\right\|\\
&\le \left\|\mathcal{S}_N\mathcal{S}_L\mathbf{U}^k - I^h\mathcal{S}_N\mathcal{S}_L\bar{\mathbf{U}}^k\right\| + C_2 h^s\left|\mathcal{S}_N\mathcal{S}_L\bar{\mathbf{U}}^k\right|_s.
\end{aligned} \tag{33}$$

Using the lemmas 3.1-3.3, the first term on the right-hand side of the formula (33) can be estimate

$$\begin{aligned}
&\left\|\mathcal{S}_N\mathcal{S}_L\mathbf{U}^k - I^h\mathcal{S}_N\mathcal{S}_L\bar{\mathbf{U}}^k\right\|\\
&\le \left\|\mathcal{S}_N\mathcal{S}_L\mathbf{U}^k - \mathcal{S}_N I^h\mathcal{S}_L\bar{\mathbf{U}}^k\right\| + \left\|\mathcal{S}_N I^h\mathcal{S}_L\bar{\mathbf{U}}^k - I^h\mathcal{S}_N\mathcal{S}_L\bar{\mathbf{U}}^k\right\|\\
&\le \left\|\mathcal{S}_L\mathbf{U}^k - I^h S_L\bar{\mathbf{U}}^k\right\| + C_3\tau(\tau^2 + h^2 + \tau h^{2+s})\\
&\le \left\|\mathcal{S}_L\mathbf{U}^k - \mathcal{S}_L I^h\bar{\mathbf{U}}^k\right\| + \left\|\mathcal{S}_L I^h\bar{\mathbf{U}}^k - I^h S_L\bar{\mathbf{U}}^k\right\|\\
&+ C_3\tau(\tau^2 + h^2 + \tau h^{2+s})\\
&\le \left\|\mathbf{U}^k - I^h\bar{\mathbf{U}}^k\right\| + C_2 h^2\left|\bar{\mathbf{U}}^k\right|_s + C_3\tau(\tau^2 + h^2 + \tau h^{2+s}).
\end{aligned} \tag{34}$$

Let $p = max\left\{\left|\bar{\mathbf{U}}^k\right|_s, \left|\mathcal{S}_N\mathcal{S}_L\bar{\mathbf{U}}^k\right|_s\right\}$, and $G = C_2 p h^2 + C_3\tau(\tau^2 + h^2 + \tau h^{2+s})$, we have

$$\left\|\mathbf{U}^{k+1} - I^h\bar{\mathbf{U}}^{k+1}\right\| \le \left\|\mathbf{U}^k - I^h\bar{\mathbf{U}}^k\right\| + G, \tag{35}$$

Finally, a combination of the above estimates, applying Gronwall inequality and $\left\|\mathbf{U}^0 - I^h\mathbf{U}^0_e\right\| = 0$, it is easy to confirm that

$$\left\|\mathbf{U}^{k+1} - I^h\mathbf{U}^{k+1}_e\right\| \le C(\tau^2 + h^2 + \tau h^{2+s} + \frac{h^s}{\tau}). \tag{36}$$

This completes the proof.

IV. Numerical experiments

In this section, in order to demonstrate the accuracy, energy stability and maximum principle of the proposed scheme for the scalar AC equation, various 2D and 3D numerical experiments are performed. We mainly adopt the periodical condition for all numerical simulations, and we choose the computational domain $\Omega = [0, 1]^2$ and $\Omega = [0, 1]^3$ in 2D and 3D, respectively.

Example 4.1 The initial value is given by

$$u = 0.2sin(2\pi x)sin(2\pi y) + 0.001. \tag{37}$$

We set the fixed parameters $T = 3$, $h = \frac{1}{160}$ and the time step sizes $\tau = \frac{1}{10}, \frac{1}{20}, \frac{1}{40}, \frac{1}{80}, \frac{1}{160}$ are used. In Fig. 1, we perform the L^2 error of the numerical solution u for the scheme (14) with $\varepsilon = 0.001$ and $\varepsilon = 0.1$. It can be easily observed that the expected convergence rates for the proposed scheme is consistent with the theoretical result. In addition, we show the curves of the discrete energy and maximum principle with the parameters $T = 100$, $h = \frac{1}{80}$, $\tau = 0.0125$, $\varepsilon = 0.001$ and $\varepsilon = 0.1$ in Fig. 2 and Fig. 3, respectively. It can be confirmed that the energy value decrease with respect to time and the numerical solution u of the presented scheme approaches but does not exceed 1 as time increases.

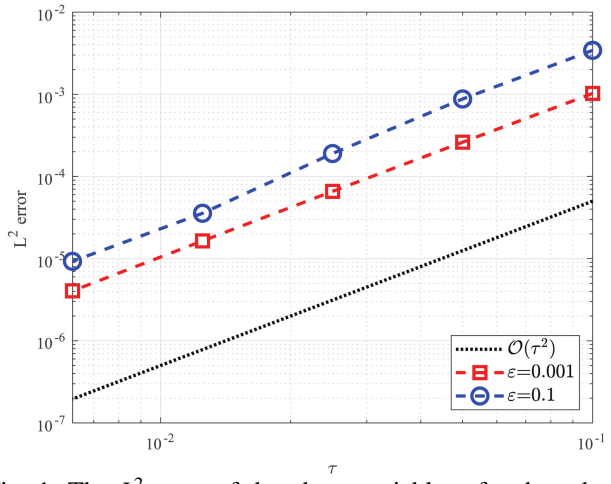

Fig. 1: The L^2 error of the phase variable u for the scheme (14) with different value of ε.

Example 4.2 In 2D case, the initial data is given by

$$u = 0.1sin(\frac{3}{2}\pi x)sin(\frac{3}{2}\pi y)cos(\pi x - 1)cos(\pi y - 1). \tag{38}$$

The parameters are set $T = 100$, $h = \frac{1}{80}$ and $\varepsilon = 0.001$. Then, we plot the discrete energy and maximum principle with different τ in Fig. 4 and Fig. 5, and show the evolutionary process of the numerical solution u in Fig. 6. It shows that the time evolution of the discrete energy is strictly non-increasing over time and the maximum value is always bounded with 1 as expected. Meanwhile, we can clearly see the process of phase separation, and finally achieve the steady state.

Example 4.3 In 3D case, we mainly choose the random initial data between -1 and 1. The parameters are set $T = 100$, $h = \frac{1}{80}$ and $\varepsilon = 0.001$. In Fig. 7, we show the maximum principle with different τ. The corresponding discrete energy

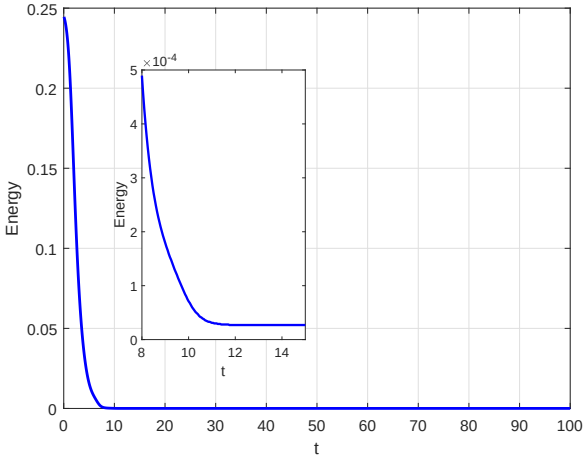

(a)

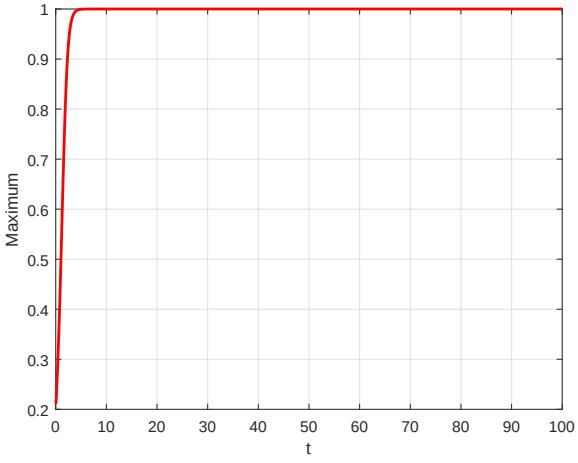

(b)

Fig. 2: The energy stability(a) and maximum principle(b) of the phase variable u for the scheme (14) with $\varepsilon = 0.001$.

are performed in Fig. 8 with different time steps τ, and the evolution of the numerical solution u in Fig. 9. In general, the presented scheme always satisfies the maximum principle and energy stability, and the evolutionary process of the phase transition are well behaved through the selection of random initial numbers, which further prove the validity and effectiveness of the presented scheme.

V. Conclusions

In this work, the exponential integrating factor method and the Strang splitting method for temporal discretization are adopted for the scalar AC equation. The key point of the paper is that the original equation is divided into linear part and nonlinear part, and the linear part is first solved analytically, the nonlinear part is solved by using the SSP-RK2 method. Therefore, we develop an effective and easy-to-implement second-order Strang splitting scheme with exponential integrating factor. The maximum principle, energy stability and convergence of the presented scheme are analyzed. Numerical results demonstrate the validity of the proposed method and the method can be applied to higher dimensional problems.

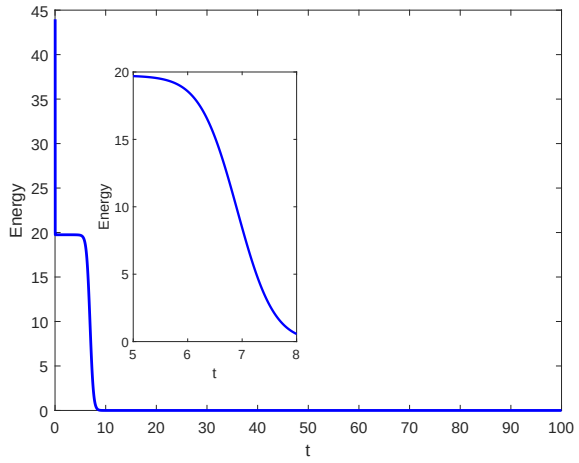

(c)

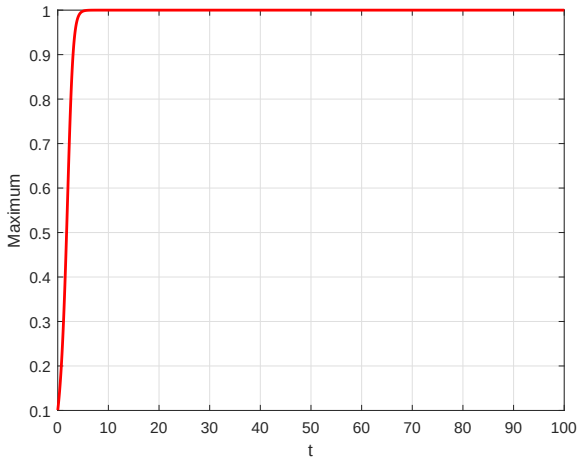

(e)

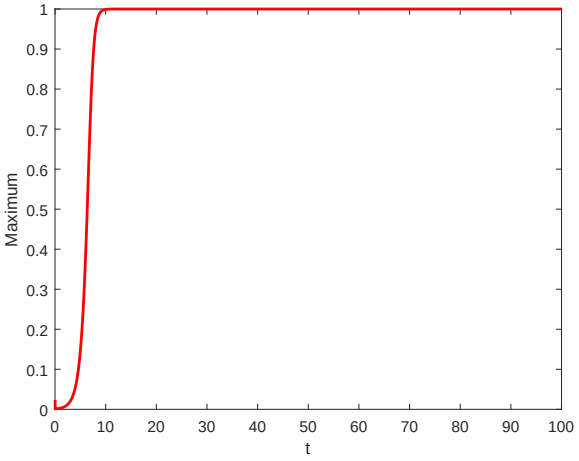

(d)

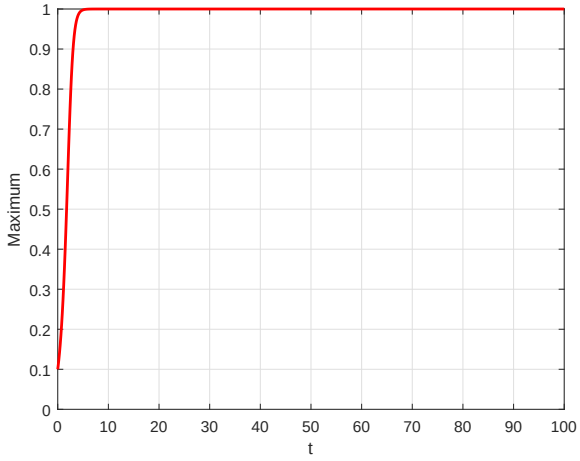

(f)

Fig. 3: The energy stability(c) and maximum principle(d) of the phase variable u for the scheme (14) with $\varepsilon = 0.1$.

Fig. 4: The verification of the maximum principle with different $\tau = 0.01$(e) and $\tau = 0.001$(f).

References

[1] S. Allen, J. Cahn, A microscopic theory for antiphase boundary motion and its application to antiphase domain coarsening, Acta Metall. 27 (1979) 1085-1095.

[2] E. Asante-Asamani, A. Kleefeld, B. Wade, A second-order exponential time differencing scheme for non-linear reaction-diffusion systems with dimensional splitting, J. Comput. Phys. 415 (2020) 109490.

[3] Q. Du, L. Ju, X. L, Z. Qiao, Maximum bound principles for a class of semilinear parabolic equations and exponential time-differencing schemes, SIAM Rev. 63 (2021) 317-359.

[4] Q. Du, L. Ju, X. Li, Z. Qiao, Maximum principle preserving exponential time differencing schemes for the nonlocal Allen-Cahn equation, SIAM J. Numer. Anal. 57 (2019) 875-898.

[5] T. Jahnke, C. Lubich, Error bounds for exponential operator splittings, BIT. 40(4) (2000) 735-744.

[6] L. Ju, X. Li, Z. Qiao, J. Yang, Maximum bound principle preserving integrating factor Runge-Kutta methods for semilinear parabolic equations, J. Comput. Phys. 439 (2021) 110405.

[7] H. Lee, J. Shin, J. Lee, First and second order operator splitting methods for the phase field crystal equation, J. Comput. Phys. 299 (2015) 82-91.

[8] D. Li, C. Quan, J. Xu, Stability and convergence of Strang splitting. Part I: Scalar Allen-Cahn equation, J. Comput. Phys. 458 (2022) 111087.

[9] J. Shen, T. Tang, J. Yang, On the maximum principle preserving schemes for the generalized Allen-Cahn equation, Commun. Math. Sci. 14 (2016) 1517-1534.

[10] J. Shen, J. Xu, J. Yang, The scalar auxiliary variable (SAV) approach for gradient flows, J. Comput. Phys. 353 (2018) 407-416.

[11] G. Strang, Accurate Partial Difference Methods II. Non-Linear Problems, Numer. Math. 6 (1964) 37-46.

[12] G. Strang, On the construction and comparison of difference schemes, SIAM J. Numer. Anal. 5(3) (1968) 506-517.

[13] S. MacNamara, S. Gilbert, Operator splitting. Splitting methods in communication, imaging, science, and engineering, Sci. Comput. Springer, Cham, (2016) 95-114.

[14] G. Marchuk, Splitting and Alternating Direction Methods, Handbook of Numerical Analysis. (1990) 197-462.

[15] T. Tang, Convergence analysis for operator-splitting methods applied to conservation laws with stiff source terms, SIAM J. Numer. Anal. 35(5) (1998) 1939-1968.

[16] T. Tang, J. Yang, Implicit-explicit scheme for the Allen-Cahn equation preserves the maximum principle, J. Comput. Math. 34 (2016) 471-481.

[17] V. Gradinaru, Strang splitting for the time-dependent Schrödinger equation on sparse grids, SIAM J. Numer. Anal. 46 (2007) 103-123.

[18] Z. Weng, Y. Deng, Q. Zhuang, S. Zhai, A fast and efficient numerical algorithm for Swift-Hohenberg equation with a nonlocal nonlinearity, Appl. Math. Lett. 118 (2021) 107170.

[19] Z. Weng, L. Tang, Analysis of the operator splitting scheme for the Allen-Cahn equation, Numer. Heat Transfer B 70 (5) (2016) 472-483.

[20] S. Zhai, Z. Weng, Y. Yang, A high order operator splitting method based on spectral deferred correction for the nonlocal viscous Cahn-Hilliard equation, J. Comput. Phys. 446 (2021) 110636.

[21] H. Zhang, J. Yan, X. Qian, S. Song, Numerical analysis and applications of explicit high order maximum principle preserving integrating factor Runge-Kutta schemes for Allen-Cahn equation, Appl. Numer. Math. 161 (2021) 372790.

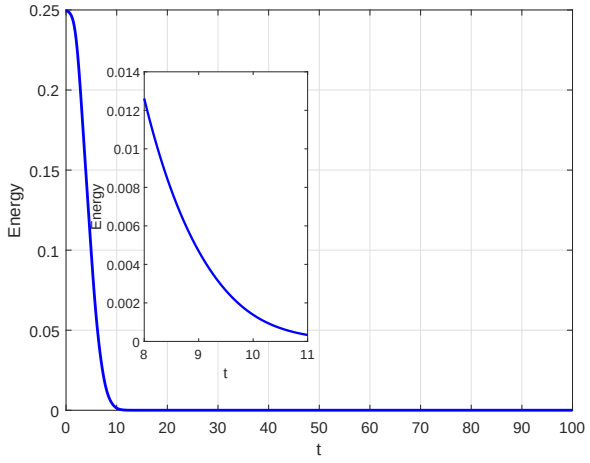

(g)

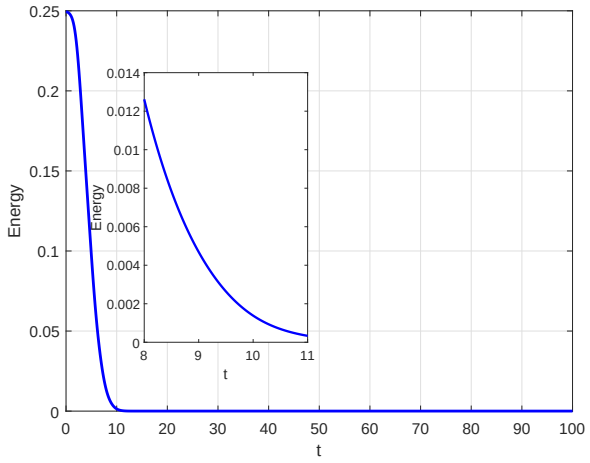

(h)

Fig. 5: The curves of the discrete energy with $\tau = 0.01$(g) and $\tau = 0.001$(h).

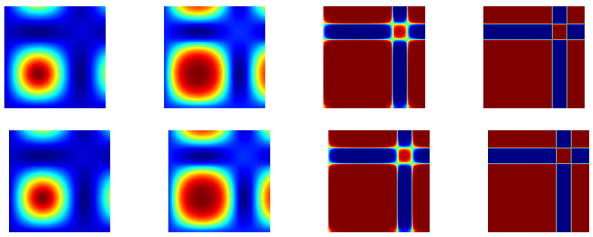

Fig. 6: The evolution of the numerical solution u in 2D with $t = 0, 3, 8, 100$ with $\tau = 0.01$(top row) and $\tau = 0.001$(bottom row).

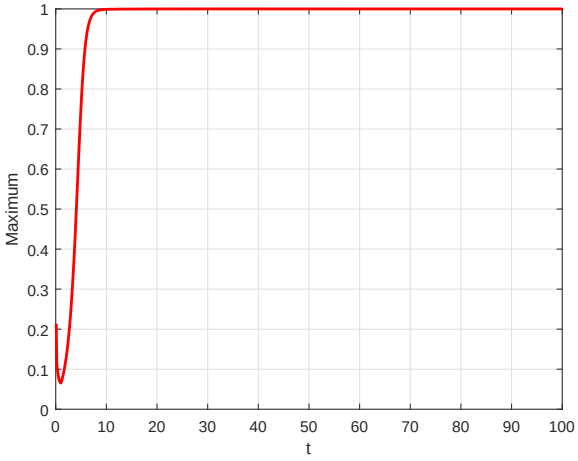

(i)

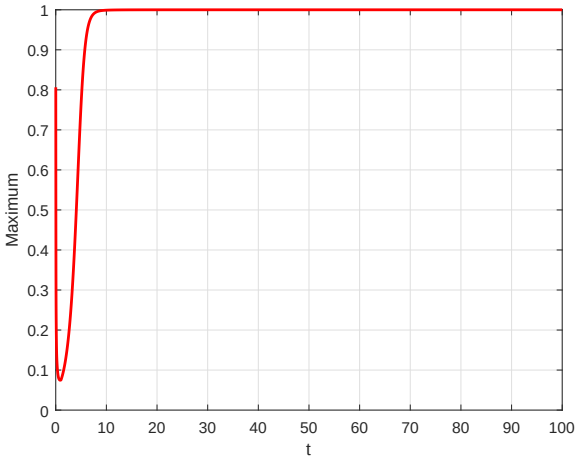

(j)

Fig. 7: The verification of the maximum principle with different $\tau = 0.1$(i) and $\tau = 0.01$(j).

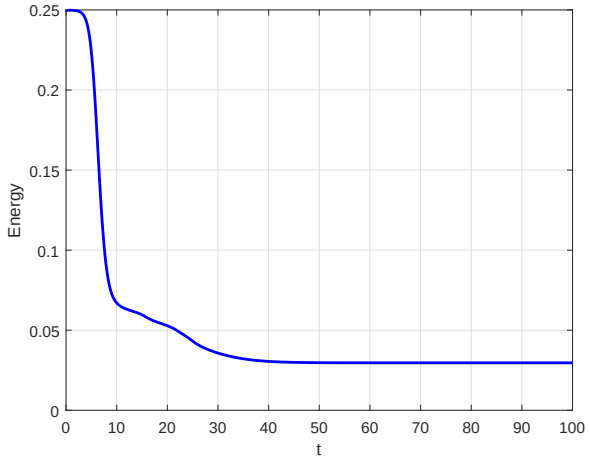

(k)

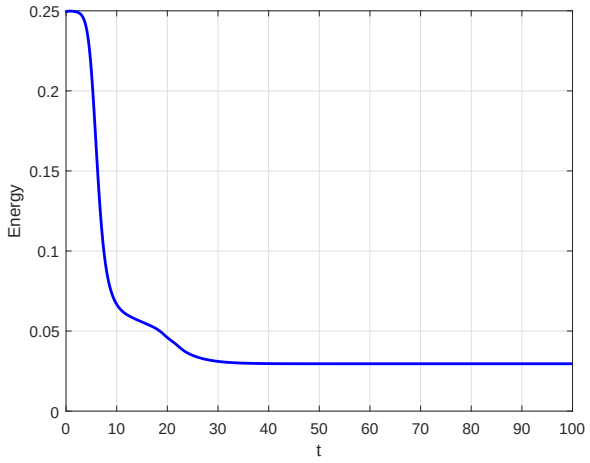

(l)

Fig. 8: The curves of the discrete energy with $\tau = 0.1$(k) and $\tau = 0.01$(l).

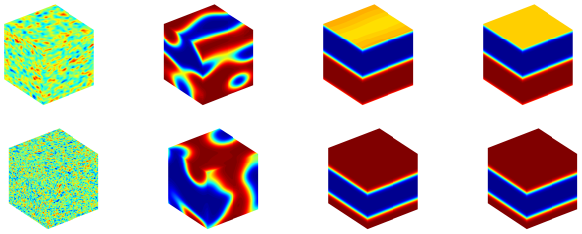

Fig. 9: The evolution of the numerical solution u in 3D with $t = 0, 10, 50, 100$ with $\tau = 0.1$(top row) and $\tau = 0.01$(bottom row).